

Phase Selection in Self-catalyzed GaAs Nanowires

Federico Panciera,* Zhaslan Baraissov, Gilles Patriarche, Vladimir G. Dubrovskii, Frank Glas, Laurent Travers, Utkur Mirsaidov,* and Jean-Christophe Harmand

Cite This: <https://dx.doi.org/10.1021/acs.nanolett.9b04808>

Read Online

ACCESS |

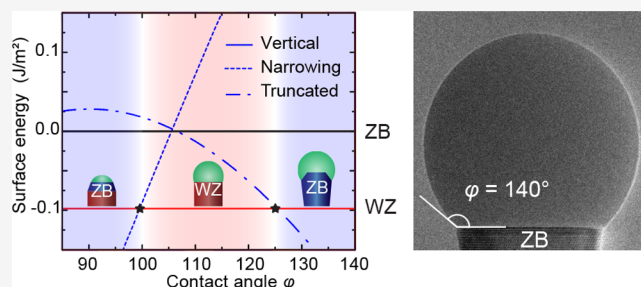
Metrics & More

Article Recommendations

Supporting Information

ABSTRACT: Crystal phase switching between the zincblende and wurtzite structures in III–V nanowires is crucial from the fundamental viewpoint as well as for electronic and photonic applications of crystal phase heterostructures. Here, the results of in situ monitoring of self-catalyzed vapor–liquid–solid growth of GaAs nanowires by molecular beam epitaxy inside a transmission electron microscope are presented. It is demonstrated that the occurrence of the zincblende or wurtzite phase in self-catalyzed nanowires is determined by the sole parameter, the droplet contact angle, which can be finely tuned by changing the group III and V fluxes. The zincblende phase forms at small ($<100^\circ$) and large ($>125^\circ$) contact angles, whereas pure wurtzite phase is observed for intermediate contact angles. Wurtzite nanowires are restricted by vertical sidewalls, whereas zincblende nanowires taper or develop the truncated edge at their top. These findings are explained within a dedicated model for the surface energetics. These results give a clear route for the crystal phase control in Au-free III–V nanowires. On a more general note, in situ growth monitoring with atomic resolution and at the technological-relevant growth rates is shown to be a powerful tool for the fine-tuning of material properties at the nanoscale.

KEYWORDS: nanowires, *in situ* TEM, crystal growth, polytypism, crystal phase



Growth of III–V semiconductor nanowires (NWs) using the vapor–liquid–solid (VLS) method can result in crystal structures different from their bulk phase.^{1–3} In GaAs NWs, for example, stable zincblende (ZB) phase coexists with metastable wurtzite (WZ) structure.⁴ Because of a relatively small difference in cohesive energy of the two phases, a modest change in the growth conditions is sufficient to switch from one phase to the other. The formation probabilities of the two phases are often close to each other, resulting in NWs having a mixed-phase structure and stacking faults. Controlling the crystal phase purity is critical for technological applications, because different crystal structures of the same chemical compound present different electronic, photonic, or phononic properties with discontinuities at their common interfaces. At the same time, controlled switching between the two phases enables synthesis of novel heterostructures with different electronic and optoelectronic properties in each phase.^{5,6} Remarkably, the valence and conduction bands of the two phases are misaligned, so that small sections of one phase within the other effectively confine charge carriers. In contrast to compositional heterojunctions, crystal phase heterostructures have intrinsically abrupt interfaces and hence do not suffer from the alloy intermixing at the interface. This feature has been proven crucial for fabrication of crystal-phase quantum dots with the exceptional properties.^{7–10}

Despite the compelling need for phase control, the lack of fundamental understanding of the governing mechanisms

prevents growing these nanostructures reliably. Several models have been proposed to date to explain the crystal phase switching. Even though the suggested mechanisms differ, there is a general consensus that the phase selection occurs at the moment of nucleation of each new monolayer (ML).¹¹ It has also been highlighted that the key parameter that determines the choice of the phase is the contact angle between the droplet and the crystal (hereafter referred to as “the contact angle”).^{11–13} A change in the contact angle alters the balance of capillary forces at the triple phase line (TPL). It may thus render the nucleation site more favorable for one phase with respect to the other. Unfortunately, despite the evident importance of controlling the contact angle, this parameter cannot be monitored or directly adjusted during growth in a standard reactor. Only the experiments conducted by in situ transmission electron microscopy (TEM)^{12,14,15} helped to shed light on the relationship between the growth parameters and the contact angle and provided valuable information for developing the droplet engineering strategies. However, these experiments treated Au-catalyzed nanowires, which are not

Received: November 20, 2019

Revised: January 13, 2020

Published: February 6, 2020

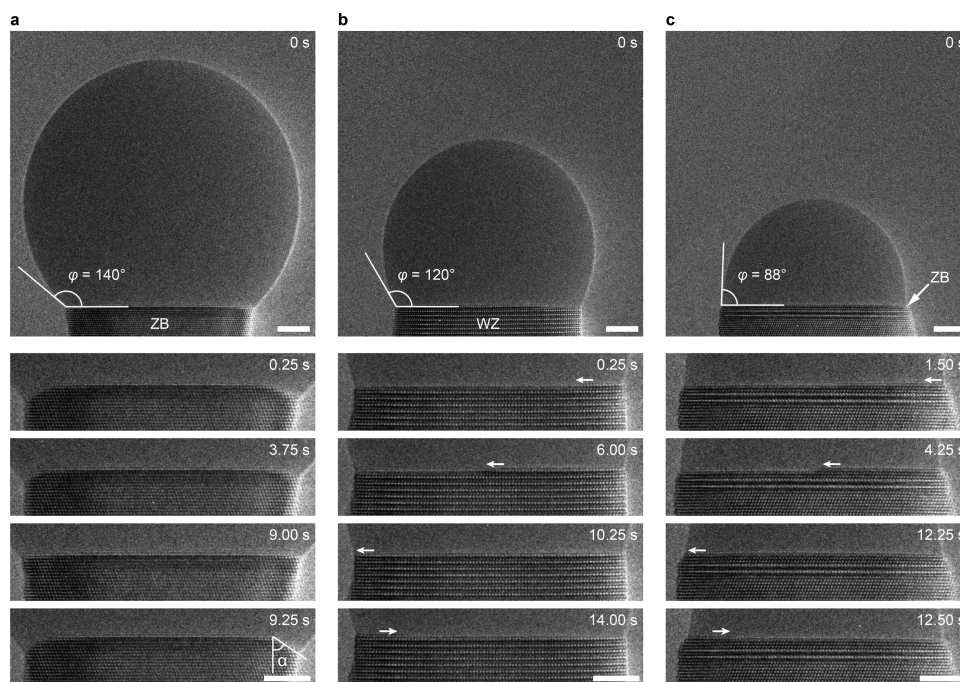


Figure 1. Growth mode and phase selection at different contact angles. All images are recorded from the same self-catalyzed GaAs NW having a diameter of ~ 30 nm and growing at 420 °C under different fluxes of As and Ga. The As/Ga flux ratio was changed during growth to tune the volume of the catalyst droplet and consequently the contact angle. Scale bars are 5 nm and the ML numbers refer to Figure 2a. (a) Images extracted from Movie 1 recorded during growth of ZB NW section (with an As flux of 0.06 nm/s and a Ga flux of 0.15 nm/s). Each new ML grows quasi-instantaneously (in one frame) and its formation corresponds to the development of the edge truncation. The truncated facet is inclined at the angle α with respect to the vertical and is wetted by the liquid catalyst. The amount of truncation oscillates with the period of ML growth, it decreases slowly but then jumps back to its maximum size with the next ML nucleation. Note that the truncation appears simultaneously on both sides of the NW; asymmetric truncations are observed in the presence of stacking faults or near the transition from ZB to WZ. The two nucleation events correspond to MLs #17 and #18. (b) Images extracted from Movie 2 (MLs #226 and #227) recorded during growth of WZ NW section (with an As flux of 0.08 nm/s and a Ga flux of 0.15 nm/s). The step flows slowly across the planar top facet of the NW; the position of the step is indicated by the arrows. (c) Images extracted from Movie 3 (MLs #377 and #378) recorded during growth of ZB NW section (with an As flux of 0.8 nm/s and Ga shutter closed). Similar to (b), the growth occurs by a slow step flow and the edge corner is sharp. The two nucleation events correspond to MLs #377 and #378.

desirable for integration with silicon platform and grown at rates much lower than in the real epitaxy systems.

Here, we present direct observations of the growth of self-catalyzed GaAs nanowires by molecular beam epitaxy (MBE) using in situ TEM. We chose to study self-catalyzed III–V NWs, as opposed to Au-catalyzed NWs,¹² due to their higher technological relevance and because this growth mode gives access to the full range of contact angles. Indeed, the droplet size can be continuously decreased until total consumption by supplying an excess of group V element. This property allows us to monitor the change of crystal phase over a wide range of contact angles and discover a mechanism for the phase transition that occurs at small angles. We show that multiple mechanisms are involved in the phase selection and develop a theoretical model to explain the observed behavior.

GaAs NWs were grown using specially designed MBE sources directly fitted on the microscope.¹⁵ The material fluxes were adjusted to obtain an average growth rate on the order of 1 ML/s, which is the typical MBE growth speed in standard systems (see Methods). By changing the ratio of Ga and As fluxes, we deliberately modified the size of the catalyst droplet and hence the contact angle. Starting from a large droplet and gradually decreasing the droplet size, the first transition from ZB to WZ is observed at a contact angle of $\sim 125^\circ$. Further decrease of the droplet size leads to the second transition, from WZ to ZB, at a contact angle of $\sim 100^\circ$.

We systematically observe three distinct regimes which are characterized by different morphologies and the formation of a specific phase. Large contact angles result in the ZB phase, where the formation of each new ML is quasi-instantaneous and the edge truncation is present at the TPL (Figure 1a). At intermediate contact angles below 125° , the WZ phase forms and the edge truncation is absent. The ML nucleates at the TPL and extends across the NW/droplet interface through a slow step flow (Figure 1b). For small contact angles below $\sim 100^\circ$, the ZB phase forms again. This second phase transition was predicted earlier to occur at contact angles well below 90° ,¹² but this was never confirmed experimentally. Remarkably, our observation reveals an important similarity between the growths of GaAs NWs at intermediate (between 100° and 125°) and small ($<100^\circ$) contact angles. In both cases, no edge truncation is observed in NWs, the ML nucleation occurs at the TPL, and lateral spreading of the ML is slow (Figure 1c). The two latter features are observed independently of the crystal phase and hence must be entirely related to the morphology of the TPL. In our conditions, the amount of As from the liquid phase is not sufficient to form the entire ML,¹⁵ thus the missing As must be supplied either from vapor or solid phase. If As is supplied from vapor, the growth duration of the full ML is limited by the As refill from vapor, which is relatively slow. This must be the case for intermediate and small contact angles, where no edge truncation is present. On the other

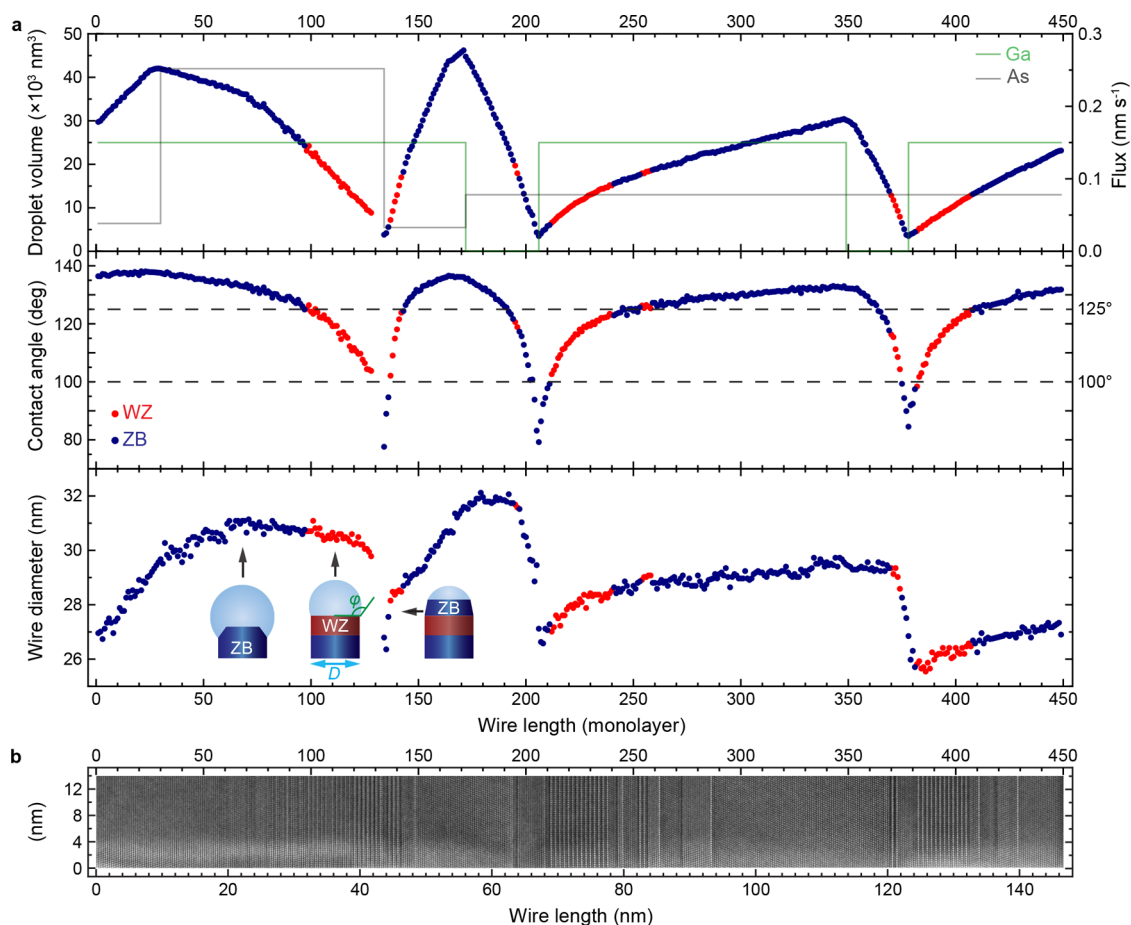


Figure 2. Time evolution of the NW morphology under varying As and Ga fluxes. (a) The droplet volume (top), contact angle (middle), and base diameter (bottom) are plotted as functions of the NW length. (b) Image of a slice of the NW obtained by composing several TEM images. Each data point is measured on the image in which the ML nucleation is observed and color-coded for the two crystal phases (blue for ZB and red for WZ). The effective fluxes of As and Ga are calculated from the axial growth rate of the NW and the change in the droplet volume (see SI paragraph S2). Data points corresponding to ML #129–133 were not recorded.

hand, if As is transferred directly from the truncated facet (whose size oscillates within the ML growth cycle), the ML can be completed quasi-instantaneously. This situation corresponds to large contact angles above 125° , where the edge truncation serves as an extra source of material for the rapid completion of the whole ML.

To understand the mechanisms for switching between these three regimes, we performed experiments in which the droplet volume was changed several times by modulating either Ga or As flux [see Supporting Information (SI), paragraphs S1 and S2 for more details]. The droplet volume can change by one of the two possible mechanisms. The first one is the change in NW diameter, where the system tends to maintain a constant contact angle. In this case, unbalanced capillary forces at the TPL lead to a change of the NW top diameter through introduction of the inclined side facets.¹⁶ Hence, the NW adjusts its diameter to keep the stable contact angle.^{17–19} The second one is the change of droplet contact angle at a constant NW diameter, leading to the phase transition when the contact angle reaches a specific critical value. Figure 2a shows that the phase transition occurs at the two critical angles, $\varphi_{\min} = 100^\circ$ and $\varphi_{\max} = 125^\circ$, regardless of whether the droplet volume is increased or decreased. Between the two critical angles, the crystal phase is WZ, switching to ZB outside this range.

This key result cannot be explained within the existing models of polytypism.^{11,12} Indeed, one central conclusion of both models is the maximum probability for the WZ phase formation at $\varphi = 90^\circ$, which contradicts our in situ data. It should be noted that these models ignore possible tapering of the NWs, which modifies the surface energy balance at the TPL.

We now consider in more detail the NW morphology to fully understand the phase switching mechanisms. Figure 2 shows that the two phases respond to the change in the droplet volume in very different ways. WZ NW maintains a constant diameter during a significant change in the contact angle (from $\varphi_{\min} = 100^\circ$ to $\varphi_{\max} = 125^\circ$). A slight increase in the top diameter visible in some cases is due to radial growth through the vertical step flow (see Movie 4), which occurs later than the axial growth and does not affect the crystal phase selection. Conversely, the diameter of ZB NW rapidly adjusts to the changing droplet volume by outward tapering (taper angle $\theta < 0$) for large or inward tapering ($\theta > 0$) for small contact angles. It is noteworthy that the phase transition from WZ to ZB occurs quasi-simultaneously with tapering of the NW. A natural question to ask is whether the phase change triggers the NW tapering or vice versa. In all of our experiments, we observed that the phase transition occurs at the same time or slightly after developing an inclined side facet in the WZ

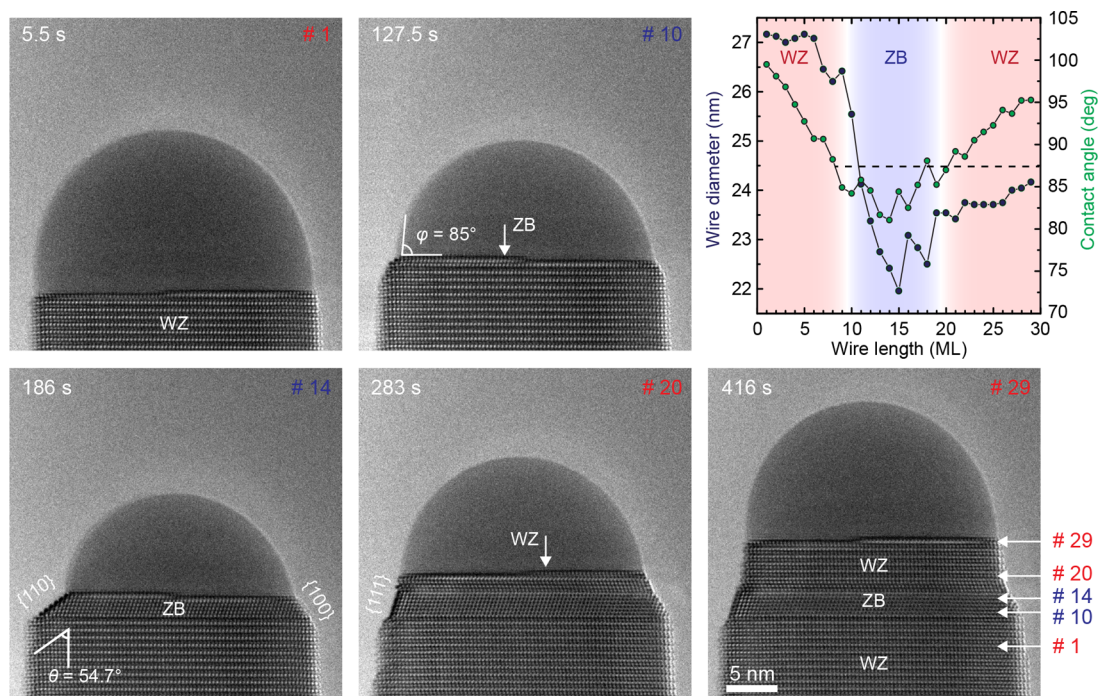


Figure 3. Sequence of images showing the phase switching caused by the NW tapering at small contact angles. Each image was captured when the ML was half-grown to make its crystal phase clearly identifiable. The graphs show the NW diameter and the contact angle versus the NW length expressed in MLs. The initial conditions are substrate temperature = 480 °C, As pressure = 1.2×10^{-5} mbar, Ga shutter closed. After ML #14, the Ga source was opened and kept at a temperature of 940 °C. When the contact angle decreases, tapering starts within the WZ phase at ML #10. When the contact angle increases, the crystal phase switches to WZ at ML #20 and simultaneously the NW sidewalls become vertical. The diameter increase after ML #14 is not caused by an inverse tapering at the interface but is rather due to radial growth which reorganizes the {110} facets into the vertical {111} facets.

Table 1. Parameter Values Used to Plot Figure 4 Based on Equations 1 and 2

model parameters	$\gamma_{(111)B}^{ZB}(w) = \gamma_{(111)B}^{ZB}(w)$ (J/m ²)	$\gamma_{(110)}^{ZB}(n) = \gamma_{(110)}^{ZB}(n)$ (J/m ²)	$\gamma_{(1\bar{1}00)}^{WZ}(v) = \gamma_{(1\bar{1}00)}^{WZ}(v)$ (J/m ²)	$\gamma_{Ga}^{LV} = \gamma_{Ga}^{LV}$ (J/m ²)	φ_{min} (deg)	φ_{max} (deg)	$\theta(w)$ (deg)	$\theta(n)$ (deg)	α (deg)	γ_{SL} (J/m ²)	γ_{AL}^{ZB} (J/m ²)
value	0.690	0.798	0.700	0.684	100	125	-19.5	54.7	54.7	0.593	0.566
source	ref ²¹	ref ²⁰	ref ²⁰	ref ²²	exp.	exp.	exp.	exp.	exp.	fit	fit

segment, as shown in Figure 3 (see also Figure S9 and Movie 4). After the phase switches to ZB, tapering proceeds by developing well-defined {110} facets (see Figure 3 and Figure S9). At small contact angles, the phase change is thus promoted by tapering the NW sidewalls.

This mechanism has some features in common with the phase change at large contact angles which, according to ref 12, is determined by developing a truncated facet at the TPL. Even though the phase switching at the two critical contact angles is governed by different mechanisms (either tapering or truncation), a unifying pattern emerges. Indeed, in both cases the phase switching from WZ to ZB is accompanied by a modification of the growth front. At the large critical angle, the side facet at the NW top changes from vertical to truncated, with the truncation inside the liquid phase, whereas at the small critical angle the side facet changes from vertical to tapered, not wetted by the liquid phase. Development of these novel inclined facets changes the surface energy balance at the TPL, which in turn determines the preferred crystal phase. The ZB phase always emerges in the presence of an inclined facet, suggesting that the edge line between the inclined facet and the top {111} facet represents the preferential nucleation site for ZB NWs. On the basis of these observations, we develop a unifying model that predicts the morphology of the growth

interface and the preferred crystal phase as a function the contact angle φ .

Generalizing the methods developed by Tersoff^{17,12} and Dubrovskii,¹⁹ we derive the two equations that represent the difference of surface energy between a given morphology, which has either tapered (t) sidewalls or truncated (tr) edges, and the reference state having vertical sidewalls and 90° edges at the TPL. In addition to the previous models, we take into account that the NW can adopt either ZB or WZ structure at the growth front and hence the solid–vapor surface energies are phase-dependent ($k = ZB$ or WZ). These equations are

$$\Delta F_t^k(\theta, \varphi) = \frac{\gamma_{\theta V}^k}{\cos \theta} - \gamma_{0V}^k - (\gamma_{SL} + \gamma_{LV} \cos \varphi) \tan \theta \quad (1)$$

$$\Delta F_{tr}^k(\alpha, \varphi) = \frac{\gamma_{\alpha L}}{\cos \alpha} - \gamma_{0V}^k - \gamma_{SL} \tan \alpha + \gamma_{LV} \sin \varphi \quad (2)$$

Here, γ_{SL} and γ_{LV} are the phase-independent surface energies of the horizontal solid–liquid and liquid–vapor interfaces; $\gamma_{\alpha L}$ is the solid–liquid surface energy of a ZB truncated facet, inclined at the angle α to the vertical; $\gamma_{\theta V}^k$ is the surface energy of vertical {110} sidewall facet of ZB NW, which represents the reference; γ_{0V}^k is the surface energy of vertical {1100} sidewall facet of WZ NW, which is lower than $\gamma_{\theta V}^k$; and $\gamma_{\theta V}^k$ is the surface

energy of a tapered facet, inclined at the angle θ to the vertical. Positive or negative angles θ correspond to narrowing or widening facets, leading to the NW tapering or inverse tapering, respectively. To model the NW morphology and phase versus the contact angle φ , we use a single set of surface energies for Ga–GaAs system gathered from the literature,^{19–23} the measured angles of the inclined facets (θ and α), and the knowledge on the phase trends deduced from our experimental observations (see Methods). By doing so, the equations contain two unknowns, the solid–liquid surface energies γ_{SL} and $\gamma_{\alpha L}$.

The curves obtained from eqs 1 and 2 are plotted by using the known surface energy values reported in Table 1 and by adjusting the two unknown values (γ_{SL} and $\gamma_{\alpha L}$) in order to fit the two critical contact angles corresponding to the ZB–WZ phase transitions. Indices “w”, “n” and “v” correspond to widening, narrowing and vertical ZB side facets, respectively. With this method, we are able to deduce the plausible values of $\gamma_{SL} = 0.593 \text{ J/m}^2$ and $\gamma_{\alpha L} = 0.566 \text{ J/m}^2$, which appear very close to each other (more details are given in SI, paragraph S4). Overall, the model explains very well our experimental observations and agrees with the earlier results. It is seen that the vertical WZ configuration is preferred for intermediate contact angles from $\varphi_{\min} = 100^\circ$ to $\varphi_{\max} = 125^\circ$, whereas for smaller and larger angles the tapered and truncated ZB configurations are more favorable. Above 125° , the growth front is truncated and the formation of WZ phase is prevented. There is a narrow range of contact angles (from 125° to 127°) where ZB NWs have vertical $\{110\}$ sidewalls, whereas for larger φ , ZB NWs exhibit inverse tapering, as often seen in self-catalyzed GaAs NWs.^{23,24} Our model also contemplates a possible formation of a truncation at very small contact angles (smaller than 55° , not shown in Figure 4), as predicted earlier

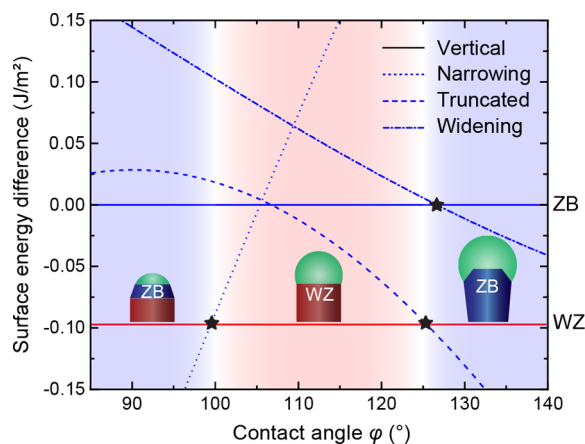


Figure 4. Model for the NW morphology and phase selection, showing the transitions from tapered ZB NWs at small contact angles to vertical WZ NWs at intermediate contact angles and back to ZB NWs with wetted truncated edges at large contact angles. Blue zero-level line corresponds to vertical $\{110\}$ ZB facets and the red horizontal line to vertical $\{1\bar{1}00\}$ WZ facets. The increasing curve for the narrowing $\{110\}$ ZB facet intercepts with the WZ one at $\varphi_{\min} = 100^\circ$, corresponding to the preferred ZB structure below 100° . The curve for the wetted truncated facet crosses with the WZ one at $\varphi_{\max} = 125^\circ$, showing that the crystal phase is ZB above φ_{\max} . The morphology of these ZB NWs is first vertical, transitioning to inverse tapered when the contact angle further increases. In both cases, the growth front is truncated. The region between the two critical angles on the WZ line corresponds to vertical WZ NWs.

in ref 12. However, at contact angles smaller than φ_{\min} , development of the tapered nonwetted facet is more favorable and hence the truncation is suppressed. Furthermore, our experiments show that when the contact angle approaches 55° , the droplet unpins from the TPL and moves freely on the top $\{111\}$ surface (Figure S9). We found, however, that the minimum angles φ_{\min} for the WZ-to-ZB phase switching vary in a range between 85° and 100° for different experiments. We ruled out a dependence on temperature, growth rate, and wire diameter, and we attribute this variability to different sidewall structures of the NWs (see SI, paragraph S3).

Precise control of the morphology of the ZB and WZ segments in crystal phase heterostructures is crucial for various applications. In this context, the phase change at large angles has two main advantages. First, it is more predictable because it occurs in a very narrow range of angles around 125° for all of the investigated growth conditions (Figure S6). Second, it does not induce any significant change in the NW diameter, particularly if the maximum contact angle is smaller than 127° . Nevertheless, the phase change at small angles cannot be ignored as it occurs almost inevitably at the two crucial steps of NW growth. This transition should be observed at the beginning of growth,¹¹ because the droplet has a much smaller contact angle when sitting on the planar substrate surface than on top of developed NWs. It also occurs at the end of growth, when the contact angle decreases when the droplet is completely²⁵ or partially²⁶ consumed. Furthermore, formation of quantum-thin GaAs NWs requires a stage of droplet shrinking under high As fluxes, where the contact angle is small.²⁷

It is worth noticing that when the droplet volume decreases rapidly, the WZ insertion between the two ZB segments becomes very short and virtually disappears in the most extreme case (see Figure 2, ML #200). This provides a clear route for fabrication of pure ZB GaAs NWs, avoiding the phase mixing at the NW top. Previous studies²⁴ suggested that self-catalyzed GaAs NWs should be almost exclusively ZB due to a low surface energy of liquid Ga compared to Au. Our results show, however, that the WZ phase in such NWs is easily achievable under relatively high V/III ratios. Predominantly ZB phase observed previously is explained by effectively Ga-rich growth conditions employed in these works. Ga-rich environment guarantees that the Ga droplet is not consumed by an excessive As flux. On the other hand, it leads to the droplet inflation, truncated growth interface, and inverse tapering, following the described growth scenario at large contact angles.

In conclusion, our in situ growth monitoring and modeling of self-catalyzed GaAs and GaSb (see Figure S8) NWs clearly shows the crystal phase switching depending on the sole parameter, the droplet contact angle, which can easily be regulated by the incoming material fluxes. The crystal phase can be changed in a regular way from pure ZB to pure WZ with the well-controlled lengths of crystal phase segments, which gives a clear route for obtaining crystal phase heterostructures in the Au-free approach. The method can be extended to other III–V NWs and demonstrates the capability of in situ method for delicate manipulations of the morphology, crystal phase, and ultimately physical properties of nanomaterials.

METHODS

Growth. We observed the growth of GaAs NWs in situ using a Cs-corrected Titan environmental TEM (ETEM), equipped with custom-made MBE sources. These sources are highly collimated so that the evaporated material only deposits onto the sample. The substrate was a Protochips heating SiC membrane with holes of 10 μm diameter. Pure Ga and As were loaded into a boron nitride crucible and heated to about 930 and 320 $^{\circ}\text{C}$, respectively, to obtain a volumetric flux on the order of 0.3 (nm^3/s) per nm^2 , which corresponds to a growth rate of about 1 ML per second (see SI, paragraph S2). This growth rate was selected as a trade-off between realistic growth conditions for a standard reactor and a growth speed that allows recording high quality data. By keeping the source temperature constant, it was possible to adjust the flux of As through a needle valve and consequently control the growth rate. Ga was initially deposited on the substrate at a temperature of 500 $^{\circ}\text{C}$, and when the Ga droplets reached the size of 20–30 nm As was introduced and temperature decreased to 420 $^{\circ}\text{C}$ to promote the growth of NWs. Because of the polycrystalline nature of the SiC substrate, NWs started growing in arbitrary directions on the substrate or were freely suspended in vacuum in correspondence to the holes. The sample was then tilted to orient the selected NW on a specific zone axis, generally $\langle 110 \rangle$. Typical experiments were carried out at a growth rate between 0.05 and 1 ML/s, and high-resolution movies were recorded using a Gatan US1000 camera at a rate of 4 frames per second. Images were analyzed using an automated script that determines the relevant parameters such as the NW diameter, the volume of the catalyst droplet, and its contact angle (see SI paragraph S1).

Model. Equations 1 and 2 were derived from theoretical work¹⁹ and plotted in Figure 4 using the surface energy values reported in Table 1. Here, thanks to the experimental determination of the critical contact angles corresponding to the crystal phase switching and identification of different facets, we can assign accurate values to the surface energies. For the angles θ , we distinguish between narrowing (n), vertical (v), and widening (w) facets. The angle $\theta(\text{n})$ and the truncation angle α are directly measured from the TEM images. For widening of ZB GaAs NWs, we deduced that the inverse tapering proceeds by alternation of vertical (110) and outward tapered (111)B sidewall facets. Therefore, in the model we assign $\theta(\text{w})$ and the corresponding surface energy value to the (111)B facet.

ASSOCIATED CONTENT

Supporting Information

The Supporting Information is available free of charge at <https://pubs.acs.org/doi/10.1021/acs.nanolett.9b04808>.

Image processing and data extraction; calculation of Ga and As fluxes from kinetic data; calculation of Ga flux from droplet growth rate; calculation of As flux from nanowire axial growth rate; variability of critical contact angles; details of the model; additional figures, references (PDF)

Growth of ZB at large contact angles ($\varphi > 125^{\circ}$). Recorded at a frame rate of 4 fps, decimated by 2, and played at 12 fps (MP4)

Growth of WZ at intermediate contact angles ($125^{\circ} > \varphi > 100^{\circ}$). Recorded at a frame rate of 4 fps, decimated by 2, and played at 12 fps (MP4)

Growth of ZB at small contact angles ($\varphi < 100^{\circ}$). Recorded at a frame rate of 4 fps, decimated by 2, and played at 12 fps (MP4)

Transition from WZ to ZB and ZB to WZ at small contact angles. Recorded at 4 fps, decimated by 10, and played at 10 fps (MP4)

AUTHOR INFORMATION

Corresponding Authors

Federico Panciera – Université Paris-Saclay, CNRS, Centre de Nanosciences et de Nanotechnologies, 91120 Palaiseau, France; Centre for BioImaging Sciences, Department of Biological Sciences, National University of Singapore, 117557, Singapore; orcid.org/0000-0003-2455-6516; Email: federico.panciera@c2n.upsaclay.fr

Utkur Mirsaidov – Centre for BioImaging Sciences, Department of Biological Sciences and Centre for Advanced 2D Materials and Department of Physics, National University of Singapore, 117557, Singapore; orcid.org/0000-0001-8673-466X; Email: mirsaidov@nus.edu.sg

Authors

Zhaslan Baraissov – Centre for BioImaging Sciences, Department of Biological Sciences and Centre for Advanced 2D Materials and Department of Physics, National University of Singapore, 117557, Singapore; orcid.org/0000-0002-2018-982X

Gilles Patriarche – Université Paris-Saclay, CNRS, Centre de Nanosciences et de Nanotechnologies, 91120 Palaiseau, France

Vladimir G. Dubrovskii – ITMO University, 197101 St. Petersburg, Russia; orcid.org/0000-0003-2088-7158

Frank Glas – Université Paris-Saclay, CNRS, Centre de Nanosciences et de Nanotechnologies, 91120 Palaiseau, France; orcid.org/0000-0002-3179-2018

Laurent Travers – Université Paris-Saclay, CNRS, Centre de Nanosciences et de Nanotechnologies, 91120 Palaiseau, France

Jean-Christophe Harmand – Université Paris-Saclay, CNRS, Centre de Nanosciences et de Nanotechnologies, 91120 Palaiseau, France

Complete contact information is available at: <https://pubs.acs.org/10.1021/acs.nanolett.9b04808>

Author Contributions

F.P., G.P., and J.-C.H. designed and conducted the experiments. Z.B., F.P., and U.M. developed the image analysis scripts and analyzed the data. V.G.D., F.P., and F.G. developed the model. J.-C.H. and L.T. developed the MBE sources. All authors have given approval to the final version of the manuscript.

Funding

We acknowledge the ANR (French National Research Agency) for funding the NanoMAX ETEM through the TEMPOS grant, project number 10-EQPX-0050 and the Singapore National Research Foundation's Competitive Research Program funding (NRF-CRP16–2015–05). V.G.D. thanks the Russian Science Foundation for financial support under the Grant 19-72-30004.

Notes

The authors declare no competing financial interest.

■ ACKNOWLEDGMENTS

We acknowledge Jean-Luc Maurice and Odile Stéphan, directors of NanoMAX and TEMPOS, respectively, for their continuous support and Ileana Florea for technical assistance.

■ REFERENCES

- (1) Koguchi, M.; Kakibayashi, H.; Yazawa, M.; Hiruma, K.; Katsuyama, T. Crystal structure change of GaAs and InAs whiskers from zinc-blende to wurtzite type. *Jpn. J. Appl. Phys.* **1992**, *31* (7R), 2061–2065.
- (2) Algra, R. E.; Verheijen, M. A.; Borgström, M. T.; Feiner, L.-F.; Immink, G.; van Enkevort, W. J.; Vlieg, E.; Bakkers, E. P. Twinning superlattices in indium phosphide nanowires. *Nature* **2008**, *456* (7220), 369–372.
- (3) Güniat, L.; Caroff, P.; Fontcuberta i Morral, A. Vapor phase growth of semiconductor nanowires: key developments and open questions. *Chem. Rev.* **2019**, *119*, 8958–8971.
- (4) Persson, A. I.; Larsson, M. W.; Stenström, S.; Ohlsson, B. J.; Samuelson, L.; Wallenberg, L. R. Solid-phase diffusion mechanism for GaAs nanowire growth. *Nat. Mater.* **2004**, *3* (10), 677–681.
- (5) Murayama, M.; Nakayama, T. Chemical trend of band offsets at wurtzite/zinc-blende heterocrystalline semiconductor interfaces. *Phys. Rev. B: Condens. Matter Mater. Phys.* **1994**, *49* (7), 4710–4724.
- (6) Spirkoska, D.; Arbiol, J.; Gustafsson, A.; Conesa-Boj, S.; Glas, F.; Zardo, I.; Heigoldt, M.; Gass, M. H.; Bleloch, A. L.; Estrade, S.; Kaniber, M.; Rossler, J.; Peiro, F.; Morante, J. R.; Abstreiter, G.; Samuelson, L.; Fontcuberta i Morral, A. Structural and optical properties of high quality zinc-blende/wurtzite GaAs nanowire heterostructures. *Phys. Rev. B: Condens. Matter Mater. Phys.* **2009**, *80* (24), 245325.
- (7) Akopian, N.; Patriarche, G.; Liu, L.; Harmand, J.-C.; Zwiller, V. Crystal phase quantum dots. *Nano Lett.* **2010**, *10* (4), 1198–1201.
- (8) Taherkhani, M.; Willatzen, M.; Mørk, J.; Gregersen, N.; McCutcheon, D. P. Type-II quantum-dot-in-nanowire structures with large oscillator strength for optical quantum gate applications. *Phys. Rev. B: Condens. Matter Mater. Phys.* **2017**, *96* (12), 125408.
- (9) Loitsch, B.; Winnerl, J.; Grimaldi, G.; Wierzbowski, J.; Rudolph, D.; Morkötter, S.; Döblinger, M.; Abstreiter, G.; Koblmüller, G.; Finley, J. J. Crystal phase quantum dots in the ultrathin core of GaAs–AlGaAs core–shell nanowires. *Nano Lett.* **2015**, *15* (11), 7544–7551.
- (10) Assali, S.; Lähnemann, J.; Vu, T. T. T.; Jöns, K.; Gagliano, L.; Verheijen, M. A.; Akopian, N.; Bakkers, E. P.; Haverkort, J. E. Crystal phase quantum well emission with digital control. *Nano Lett.* **2017**, *17* (10), 6062–6068.
- (11) Glas, F.; Harmand, J.-C.; Patriarche, G. Why does wurtzite form in nanowires of III-V zinc blende semiconductors? *Phys. Rev. Lett.* **2007**, *99* (14), 146101.
- (12) Jacobsson, D.; Panciera, F.; Tersoff, J.; Reuter, M. C.; Lehmann, S.; Hofmann, S.; Dick, K. A.; Ross, F. M. Interface dynamics and crystal phase switching in GaAs nanowires. *Nature* **2016**, *531* (7594), 317–322.
- (13) Dastjerdi, M.; Boulanger, J.; Kuyanov, P.; Aagesen, M.; LaPierre, R. Methods of Ga droplet consumption for improved GaAs nanowire solar cell efficiency. *Nanotechnology* **2016**, *27* (47), 475403.
- (14) Panciera, F.; Norton, M. M.; Alam, S. B.; Hofmann, S.; Mølhav, K.; Ross, F. M. Controlling nanowire growth through electric field-induced deformation of the catalyst droplet. *Nat. Commun.* **2016**, *7*, 12271.
- (15) Harmand, J.-C.; Patriarche, G.; Glas, F.; Panciera, F.; Florea, I.; Maurice, J.-L.; Travers, L.; Ollivier, Y. Atomic step flow on a nanofacet. *Phys. Rev. Lett.* **2018**, *121* (16), 166101.
- (16) Schwarz, K.; Tersoff, J. Elementary processes in nanowire growth. *Nano Lett.* **2011**, *11* (2), 316–320.
- (17) Schwarz, K.; Tersoff, J.; Kodambaka, S.; Chou, Y.-C.; Ross, F. Geometrical frustration in nanowire growth. *Phys. Rev. Lett.* **2011**, *107* (26), 265502.
- (18) Krogstrup, P.; Popovitz-Biro, R.; Johnson, E.; Madsen, M. H.; Nygård, J.; Shtrikman, H. Structural phase control in self-catalyzed growth of GaAs nanowires on silicon (111). *Nano Lett.* **2010**, *10* (11), 4475–4482.
- (19) Dubrovskii, V. Development of growth theory for vapor–liquid–solid nanowires: contact angle, truncated facets, and crystal phase. *Cryst. Growth Des.* **2017**, *17* (5), 2544–2548.
- (20) Pankoke, V.; Kratzer, P.; Sakong, S. Calculation of the diameter-dependent polytypism in GaAs nanowires from an atomic motif expansion of the formation energy. *Phys. Rev. B: Condens. Matter Mater. Phys.* **2011**, *84* (7), 075455.
- (21) Moll, N.; Kley, A.; Pehlke, E.; Scheffler, M. GaAs equilibrium crystal shape from first principles. *Phys. Rev. B: Condens. Matter Mater. Phys.* **1996**, *54* (12), 8844–8855.
- (22) Dubrovskii, V.; Sibirev, N.; Cirilin, G.; Soshnikov, I.; Chen, W.; Larde, R.; Cadel, E.; Pareige, P.; Xu, T.; Grandidier, B. Gibbs–Thomson and diffusion-induced contributions to the growth rate of Si, InP, and GaAs nanowires. *Phys. Rev. B: Condens. Matter Mater. Phys.* **2009**, *79* (20), 205316.
- (23) Rudolph, D.; Hertenberger, S.; Bolte, S.; Paosangthong, W.; Spirkoska, D.; Döblinger, M.; Bichler, M.; Finley, J. J.; Abstreiter, G.; Koblmüller, G. Direct observation of a noncatalytic growth regime for GaAs nanowires. *Nano Lett.* **2011**, *11* (9), 3848–3854.
- (24) Dubrovskii, V. G.; Cirilin, G.; Sibirev, N.; Jabeen, F.; Harmand, J.-C.; Werner, P. New mode of vapor–liquid–solid nanowire growth. *Nano Lett.* **2011**, *11* (3), 1247–1253.
- (25) Plissard, S.; Dick, K. A.; Larrieu, G.; Godey, S.; Addad, A.; Wallart, X.; Caroff, P. Gold-free growth of GaAs nanowires on silicon: arrays and polytypism. *Nanotechnology* **2010**, *21* (38), 385602.
- (26) Lehmann, S.; Jacobsson, D.; Dick, K. A. Crystal phase control in GaAs nanowires: opposing trends in the Ga- and As-limited growth regimes. *Nanotechnology* **2015**, *26* (30), 301001.
- (27) Kim, W.; Dubrovskii, V. G.; Vukajlovic-Plestina, J.; Tütüncüoğlu, G.; Francaviglia, L.; Güniat, L.; Potts, H.; Friedl, M.; Leran, J.-B.; Fontcuberta i Morral, A. Bistability of contact angle and its role in achieving quantum-thin self-assisted GaAs nanowires. *Nano Lett.* **2018**, *18* (1), 49–57.